Scientific paper

Binding Sites of Deprotonated Citric Acid and Ethylenediaminetetraacetic Acid in the Chelation with Ba^{2+}, Y^{3+}, and Zr^{4+} and Their Electronic Properties: a Density Functional Theory Study

Nor Ain Fathihah Abdullah and Lee Sin Ang*

Faculty of Applied Sciences (Physics), Universiti Teknologi MARA Cawangan Perlis, 02600 Arau, Malaysia

** Corresponding author: E-mail: anglee631@perlis.uitm.edu.my*
Tel: +604 98 82 573

Received: 02-10-2017

Abstract

Density functional calculations were performed on the metal complexes formed during the synthesis of barium zirconate (BZY). This compound has been synthesized previously, but the molecular interactions present during the formation of the ligand–metal complexes are unknown. In this study, calculations were carried out to determine the preferred coordination sites for the metal complexes. The cations Ba^{2+}, Y^{3+}, and Zr^{4+} were modeled to interact with two deprotonated chelating agents (citric acid [CA] and ethylenediaminetetraacetic acid [EDTA]) at strategic positions. Density functional theory (DFT) at the B3LYP level of theory with basis set 6-31G* and Universal Gaussian Basis Set (UGBS) was used. The relevant geometries, binding energies, and charge distributions of the complexes are reported. It was found that both CA and EDTA can bind the metal cations investigated in this study. Metal cations prefer to form bonds at the electron-rich sites of the chelating agents. Of the three metal cations considered, Zr^{4+} was found to possess the strongest bonds to deprotonated CA and EDTA, followed by Y^{3+} and then Ba^{2+}.

Keywords: Density functional theory, cations, chelating agents, binding energies, charges

1. Introduction

Currently, perovskite is one of the most studied compounds in the field of materials science.[1–3] Ceramic perovskite-type oxides, with a general formula ABO_3 where A and B are two metal cations of different sizes, have been studied due to their high conductivity and low activation energy.[4,5] Cerate zirconate attracts much attention among perovskite-type oxides because it is important for the future development of electrochemical devices such as fuel cells, magnetic refrigeration, and solar cells.[6–8] Perovskite can be synthesized at low cost as it can be made from common metals and industrial chemicals[9] and is convenient to prepare.[7]

Many researchers have investigated the role of the chelating agents in the formation of perovskite.[10–12] As the formation of perovskite involves the complexation process, the interaction between the metal and chelating agent is of utmost importance. Liu et al[12] identified that citric acid (CA) is more effective than ethylenediaminetetraacetic acid (EDTA) in forming perovskite at low temperatures (<1000 °C). When the chelating agents are used together, the combined CA and EDTA increases the chelating strength to the metal ion, as demonstrated in a study by Osman et al[11] in which the CA and EDTA were mixed into a metal nitrate solution to form metal–CA–EDTA complexes with a ratio of 2:1:1. A similar effect was also observed by Tao et al[13] in the synthesis of $La_{0.6}Sr_{0.4}CoO_{3-\delta}$. CA has three carboxyl groups that can bind with metal cations whereas EDTA has four carboxyl and two amine groups, demonstrating that the strength of the chelating agents affects the interactions during the chelation process.[12,14]

Despite previous research showing that the use of chelating agents provides a good platform for the production of perovskites, the molecular interactions involved are still unclear. The microscopic behaviors and characteristics of the intermediate structures, as well as the ligand–metal complexes, are unknown. Furthermore, research into the microscopic properties of metal cation complexation with chelating agents is scarce.

Several theoretical studies into the favored sites for complexation have been carried out to find the most stable structure in the intermediate state.[15–17] Primikyri et al[15] performed DFT studies on the chelation of Zn to quercetin and luteolin in their neutral and deprotonated forms. It was found that the preferred cation bonding sites were in between the carbonyl and deprotonated hydroxyl groups of quercetin and luteolin. This is in line with the work reported by Leopoldini et al.[16] The preference of metal cations to form complexes at these sites is due to the lone pairs of electrons from the O atoms at the carbonyl and deprotonated hydroxyl groups.

In this study, we intended to confirm the important initial step involved in the one-pot synthesis of barium zirconate (BZY). Metal cations Y^{3+}, Ba^{2+}, and Zr^{4+} were modeled to combine with two chelating agents, CA and EDTA. DFT was employed to determine the interactions between the chelating agents and the metal cations at the microscopic level. This included possible metal cation attachment sites and the electronic structure of the complexes formed. This study focusses only on the interaction between metal and chelating agent with a ratio of 1:1, therefore the effects of coordination sphere saturation in the metal ions has not been discussed.

2. Computational Details

In a previous study, $Ba(NO_3)_2$, $Zr(NO_3)_2O.xH_2O$, and $Y(NO_3)3.5H_2O$ were dissolved to produce the metal cations and form the metal–chelating agent complexes.[11] In order to portray correctly the charge state of the metal cations, they have been modeled as having the indicated positive charges in the calculations. To further facilitate the calculations, the existence of Zr^{4+} in the one-pot synthesis is approximated.

The structures of chelating agents CA and EDTA were obtained from the Chemspider database.[18] CA and EDTA were deprotonated at the carboxylic acid groups (COOH), making them negatively charged as in the real system these protons would be dissociated. The deprotonated chelating agents were labeled as CA_{3H} and $EDTA_{4H}$. The metal cations were then attached to the chelating agents at five positions labeled P1 to P5. These positions are shown in Fig. 1.

All calculations were carried out using the Gaussian 09 suite of programs.[19] The B3LYP functional with dual basis sets 6-31G* for C, O, N, and H atoms and Universal Gaussian Basis Set (UGBS) for metal cations was used. The D3 version of Grimme's dispersion correction with Becke-Johnson (BJ) damping was adopted in the metal-complex calculations[20,21] to improve the dispersion energy in the B3LYP method. All the results were visualized using GaussView[22] and Chem3D molecular modeling software.

The binding energy (E_b) was used to compute the stability of the complexes. The E_b of the metal complexes was calculated from the expression:[23]

$$E_b = E_{M\text{-complex}} - E_M - E_{chelate} \quad (1)$$

where $E_{M\text{-complex}}$ is the energy of the metal and chelating agent, $E_{chelate}$ represents the energy of the chelating agent, and E_M is the energy of the metal cation.

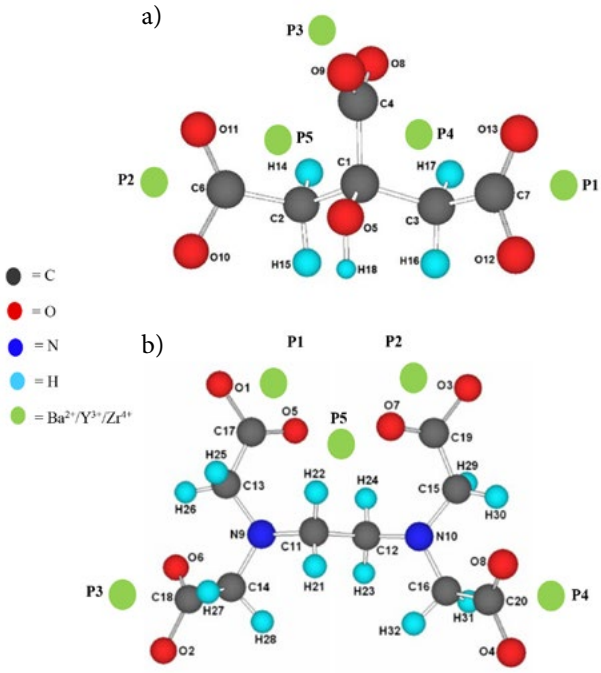

Fig. 1. Molecular structure of (a) CA_{3H} and (b) $EDTA_H$ with metal attachment (Ba^{2+}, Y^{3+}, Zr^{4+}) at different positions (P1 to P5). Metal cations are green and C, O, N, and H are colored grey, red, blue, and turquoise, respectively.

3. Results and Discussion

3. 1. Binding Energies

EDTA and CA are chelating agents that can bind to metal cations to form complexes. EDTA is a type of polyamino carboxylic acid that can bind to a metal via four carboxyl and two amine groups, meaning it has six sites with a lone pair of electrons. CA is a polydentate ligand and can bind to metals via three carboxyl groups with a lone pair of electrons at each. In this study, the binding energies of metal–CA_{3H} and metal–$EDTA_{4H}$ complexes were calculated in order to determine their stability.

At the level of theory B3LYP/6-31G* and UGBS geometry optimization, the following results were obtained: $E(CA_{3H})$ = –20626.57 eV, $E(EDTA_{4H})$ = –29911.50 eV, $E(Ba^{2+})$ = –214598.65 eV, $E(Y^{3+})$ = –90707.64 eV, and $E(Zr^{4+})$ = –96342.96 eV.

The binding energies of CA_{3H} and $EDTA_{4H}$ metal complexes were calculated from equation (1) and are shown in Tables 1 and 2. A higher negative value of E_b indicates higher stability of the complex. Table 1 shows the E_b of metal–CA_{3H} complexes at five different positions of

metal attachment. Ba^{2+} attaches strongly at P2 and has an E_b of –19.39 eV. Interestingly, in Y–CA_{3H}, the E_b is highest at P4 and P5 and both sites have the same E_b of –21.82 eV. In the Zr–CA_{3H} complex, the E_b values at P4 and P5 are similar at –24.89 eV. The highest and most stable E_b was at P3 (–25.69 eV).

The calculated E_b values of metal–$EDTA_{4H}$ complexes are tabulated in Table 2. In Ba–$EDTA_{4H}$ complexes, Ba^{2+} prefers to attach at P2 as this E_b (–26.67 eV) is the highest compared to other sites. Table 2 also shows that the E_b for P1 differs from P2 by 0.01 eV. Hence, these two sites in $EDTA_{4H}$ are favorable to Ba^{2+} for attachment. In the Y–$EDTA_{4H}$ and Zr–$EDTA_{4H}$ complexes, the cations bonded strongly at P5 and exhibited a high E_b values of –33.12 eV and –37.33 eV, respectively.

Table 1. Binding energies (E_b) of CA_{3H} complexes. Numbers in bold represent the most stable metal complexes.

Positions	E_b (eV)		
	Ba–CA_{3H}	Y–CA_{3H}	Zr–CA_{3H}
P1	–18.92	–21.65	–24.23
P2	**–19.39**	–21.65	–24.23
P3	–19.01	–21.72	**–25.69**
P4	–18.92	**–21.82**	–24.89
P5	–18.92	**–21.82**	–24.89

Table 2. Binding energies (E_b) of $EDTA_{4H}$ complexes. Numbers in bold represent the most stable metal complexes.

Positions	E_b (eV)		
	Ba–$EDTA_{4H}$	Y–$EDTA_{4H}$	Zr–$EDTA_{4H}$
P1	–26.66	–29.62	–32.31
P2	**–26.67**	–29.62	–32.31
P3	–25.71	–27.34	–28.99
P4	–17.08	–27.33	–28.96
P5	–26.56	**–33.12**	**–37.33**

The results discussed in the preceding paragraph can be explained using electrostatic potential (ESP) maps for the molecules of CA and EDTA as illustrated in Fig. 2. ESP enables visualization of charge distribution in the molecules using color codes. The red regions indicate more negative potential, while the blue regions indicate less negative potential (or positive potential). As displayed in Fig. 2 (a), the most negative potential is distributed around P4 and P5, in between the central carboxyl group and on the carboxyl groups at either end of the CA molecule. These groups are susceptible to electrophilic attack, hence Ba^{2+}, Y^{3+}, and Zr^{4+} prefer to bind to CA at these two positions. EDTA has four carboxyl and two amine groups susceptible to electrophilic attack, therefore these sites have a high possibility of metal complexation (in Fig. 2 (b), these sites are shown in orange). As can be seen in Table 2, the binding energies are low at P3 and P4 compared to other positions due to the low negative potential.

At each preferred site, the Ba complexes have the smallest E_b values compared to the other metal complexes. The larger size of Ba^{2+} makes it less stable and prevents the ligand from chelating completely.[24–26] Zr^{4+} complexes exhibit higher E_b values than Y^{3+} complexes despite being larger in size. The ionic charge for Zr^{4+} is larger than for Y^{3+} and the stability of the metal complex decreases with decreasing ionic charge.[24,27] These results are supported by Bohm et al[28] in that the interaction energy increases as the size of the metal decreases, $K^+ > Na^+ > Li^+$ with values of –5.65 eV, –8.71 eV, and –12.05 eV, respectively.

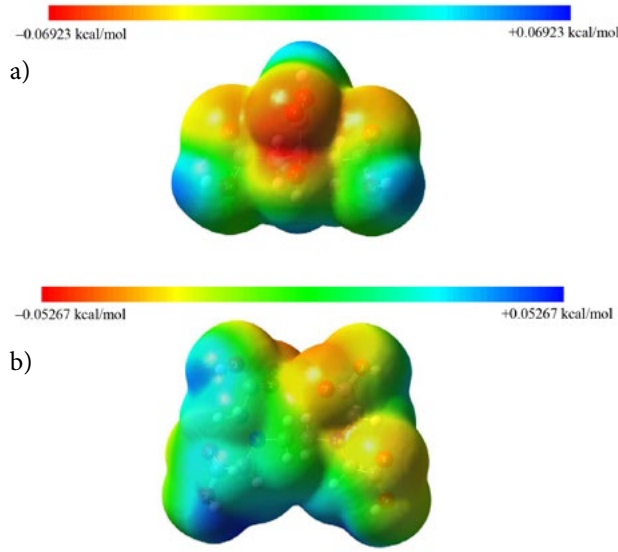

Fig. 2. The electrostatic potential map of (a) CA and (b) EDTA. Isovalue of electron density = 0.0002 au (e/a_o^3). Refer to figure 1 for the structures without the isosurface.

Based on Tables 1 and 2, similar E_b values are observed at P1/P2 and P4/P5 in Y–CA_{3H} and Zr–CA_{3H} complexes. This is due to the symmetrical arrangement of the atoms in CA. However, this is not observed in Ba–CA_{3H}, potentially due to the larger size of Ba^{2+}. Similarly in the Ba–$EDTA_{4H}$ complex, it is difficult for Ba^{2+} to reside at any other site on EDTA due to its larger size.

3. 2. Geometry Optimization

Geometry optimizations were performed on the metal complexes using 6-31G* and UGBS basis sets and no imaginary frequencies were observed. The stationary point of each structure where the energy was at a minimum was therefore ascertained.[29] The geometrically optimized structures of the most stable metal–CA_{3H} and metal–$EDTA_{4H}$ complexes formed are shown in Fig. 3 to 8. The

bond lengths between metal and O are discussed since O and N donate electrons and play an important role in the metal interaction.

In general, metal complexation marginally changes the shape of CA_{3H}. Ba^{2+} was found most stable at P2 with bond lengths of Ba–O5 = 2.704 Å, Ba–O9 = 2.602 Å, and Ba–O11 = 2.602 Å (the optimized structure of Ba–CA_{3H} is shown in Fig. 3). These results concur with findings from a previous study by Makrlik et al[30] where the bond length of Ba^{2+} to oxygen atoms in the beauvericin ligand are 2.5~4.9 Å.

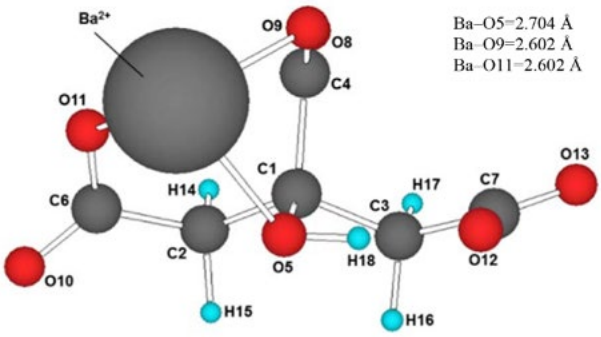

Fig. 3. Optimized structure of the most stable Ba–CA_{3H} complex (P2)

Y^{3+} was found to be the most stable at equivalent sites P4 and P5 (Fig. 4). The cation bonds to three O atoms, two from the carboxyl group and one from the hydroxyl group. The bond lengths obtained for Y–O9 at P4 and P5 are 2.160 Å. Y–O13 and Y–O11 at P4 and P5, respectively, also had the same bond length at 2.155 Å. The bond length observed for Y–O5 at P4 and P5 differed by 0.001 Å. This small difference in bond length is negligible. These were in accordance with the Y-O bond lengths observed in a previous study.[31]

As depicted in Fig. 5, Zr^{4+} favored P3 in the Zr-CA_{3H} complex. Zr^{4+} is bonded to three O atoms (O8, O9, and O11) on the carboxyl groups of CA_{3H}. The bond lengths for Zr–O8, Zr–O9, and Zr–O11 are 2.035 Å, 2.021 Å, and 2.009 Å, respectively. Similar bond lengths were recorded by Vlaic et al[32] where bond lengths of Zr-O in Rh/$Ce_{0.5}Zr_{0.5}O_2$ were 1.11~2.34 Å. The most stable sites in Ba-CA_{3H}, Y-CA_{3H}, and Zr-CA_{3H} were observed between carboxyl and hydroxyl groups and this is in accordance with results reported by Primikyri et al[15] and Leopoldini et al.[16]

Figs 6 to 8 show the optimized structure of the most stable metal–$EDTA_{4H}$ complexes. There were significant changes to the shape of $EDTA_{4H}$ after metal complexation. EDTA is able to form bonds with any metal and its chela-

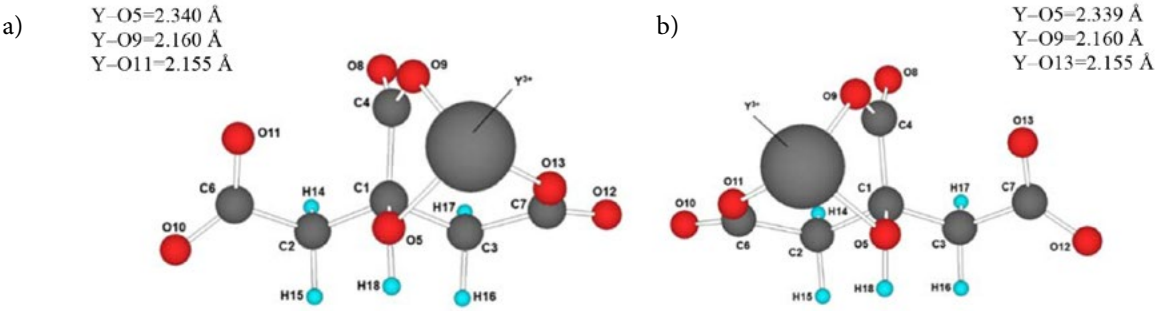

Fig. 4. Optimized structure of the most stable Y–CA_{3H} complex at (a) P4 (b) P5

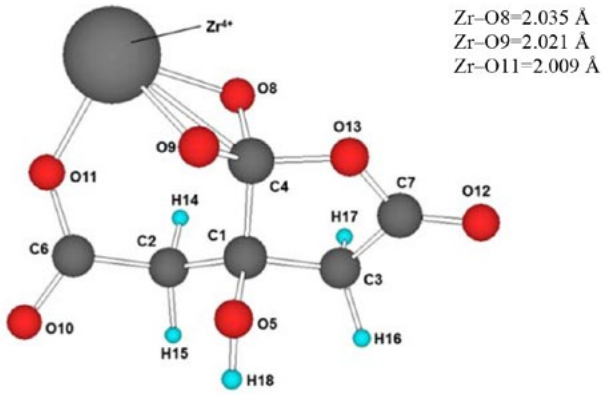

Fig. 5. Optimized structure of the most stable Zr–CA_{3H} complex (P3)

tion depends on the size and ionic charge of the metal cation.[33] The most stable geometrical structure of metal–EDTA$_{4H}$ shows carboxyl O atoms and N atoms moving closer to the metal cation, almost encasing it. Both O and N atoms are able to create bonds with the metal cations as they consist of a lone pair electron.

In the optimized structure of the Ba-EDTA$_{4H}$ complex shown in Fig 6, Ba^{2+} is found to be the most stable at P2. Ba^{2+} bonds to the four nearest O atoms from the carboxyl groups with bond lengths of Ba-O1, Ba–O3, Ba-O5, and Ba–O7 are 2.764 Å, 2.750 Å, 2.710 Å and 2.725 Å, respectively. Furthermore, the geometrical structure of Ba–EDTA$_{4H}$ was similar to the original structure before the addition of Ba^{2+}. Several experimental studies encountered problems with $BaCO_3$ impurities after synthesizing a single layer of perovskites, due to the use of EDTA as the chelating agent.[11,34] In other reports, triethylenetetraamine (TETA) has been shown to help solve the problem of $BaCO_3$ impurities at a lower temperature.[10,35] This may be due to the ability of chelating agents to bind with Ba^{2+}. It can be concluded that Ba^{2+} is effectively complexed by the amine group.

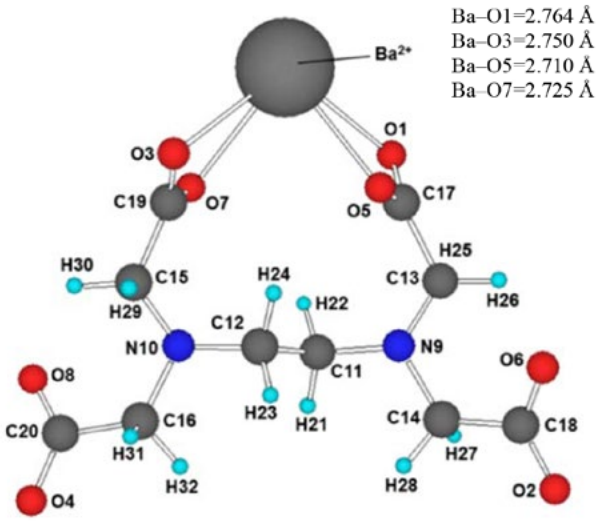

Fig. 6. Optimized structure of the most stable Ba–EDTA$_{4H}$ complex (P2)

From Fig. 7 shows that Y^{3+} is embraced by EDTA$_{4H}$. A similar geometry was found by Thomas et al[36] in an investigation into the molecular structure of aqueous Hg(II)-EDTA. Unlike the Ba-EDTA$_{4H}$ complex, the four carboxyl O atoms and two N atoms in EDTA$_{4H}$ bind strongly to Y^{3+} due to its smaller size, making it easy to be caught by the EDTA ligand. The bond lengths for Y–EDTA$_{4H}$ are as follows: Y–O5 = 2.273 Å, Y–O6 = 2.297 Å, Y–O7 = 2.273 Å, Y–O8 = 2.297 Å, Y–N9 = 2.528 Å, and Y–N10 = 2.527 Å. These bond lengths are consistent with Y-O and Y-N bond lengths observed previously in the formation of guanidinate yttrium complexes.[31]

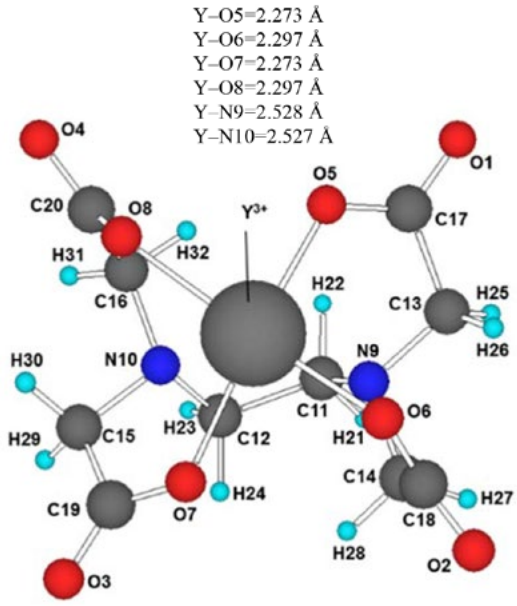

Fig. 7. Optimized structure of the most stable Y–EDTA$_{4H}$ complex (P5)

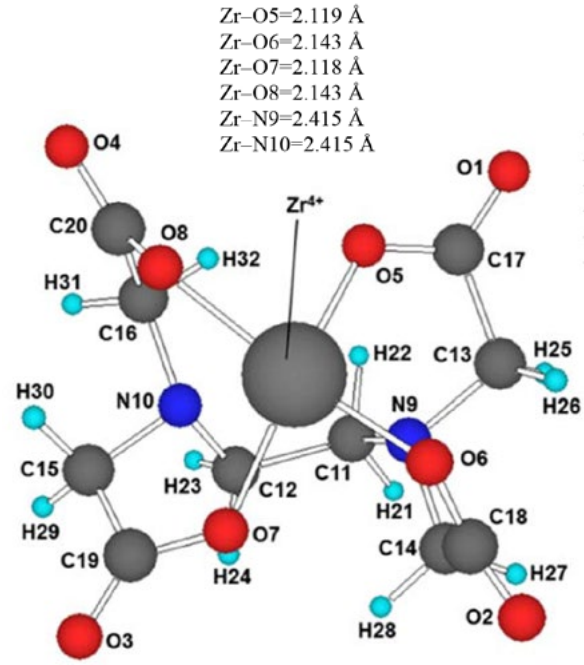

Fig. 8. Optimized structure of the most stable Zr–EDTA$_{4H}$ complex (P5)

Zr^{4+} was similarly encased by EDTA$_{4H}$ at P5 in the Zr–EDTA$_{4H}$ complex (Fig. 8). Zr^{4+} was bonded to four carboxyl groups and two amine groups from EDTA$_{4H}$. EDTA$_{4H}$ is able to strongly wrap around metal cations due to lone pairs of electrons from two types of ligand (carboxyl and amine groups). The interaction between Zr^{4+} and EDTA$_{4H}$ is the strongest with bond lengths of Zr–O5 = 2.119 Å, Zr–O6 = 2.143 Å, Zr–O7 = 2.118 Å, Zr–O8 =

2.143 Å, Zr–N9 = 2.415 Å, and Zr–N10 = 2.415 Å. The bond lengths measured were in agreement with findings by Suzuki et al,[37] where the bond length of Zr–O in [Zr (CO_3)EDTA]$^{2+}$ was determined. Similarly, the bond length is in accordance with findings by Pozhidaev et al[38] where the bond length of Zr–O in the crystal structure of Zr–ethylenediaminetetracetate tetrahydrate was measured to within a range of 2.1~2.3 Å, and Zr–N was 2.43 Å.

3. 3. Mulliken Charges

The Mulliken charges of the most stable metal–CA_{3H} and metal–$EDTA_{4H}$ complexes are shown in Tables 3 and 4. The initial ionic charges of Ba^{2+}, Y^{3+}, and Zr^{4+} decrease after complexation with CA_{3H} and $EDTA_{4H}$. The decreasing in charge can be attributed to the transfer of electrons from CA and EDTA to the metal.[39,40] The charge transfer in metal complexes is of utmost important as it influences the interaction between metal and chelating agent. It can be inferred that the greater the charge reduction in the metal the stronger the interaction in the metal complex.[41]

Table 3. Charge of metals after complexation with the chelating agent.

Metals	Mulliken atomic charge of metals in metal complexes		
	Initial	After optimized (CA_{3H})	After optimized ($EDTA_{4H}$)
Ba	+2	+1.544	+1.508
Y	+3	+2.104	+1.449
Zr	+4	+2.672	+1.911

The C atoms, C2 and C3 in CA_{3H} and C11 to C16 in $EDTA_{4H}$ (Table 4), carry negative charges as they are bonded to C and N atoms, respectively. Both atoms attract the bonding pair of electrons to exactly the same extent. That

Table 4. Mulliken charges of the most stable metal–CA_{3H} complexes

Complexes	Atom charges						
	C1	**C2**	**C3**	**C4**	**C6**	**C7**	
Ba–CA_{3H}	0.259	–0.367	–0.389	0.511	0.515	0.495	
Y–CA_{3H}	0.215	–0.398	–0.389	0.621	0.587	0.490	
Zr–CA_{3H}	0.181	–0.398	–0.407	0.666	0.627	0.534	
	O5	**O8**	**O9**	**O10**	**O11**	**O12**	**O13**
Ba–CA_{3H}	–0.780	–0.597	–0.675	–0.593	–0.669	–0.632	–0.601
Y–CA_{3H}	–0.739	–0.523	–0.688	–0.511	–0.682	–0.631	–0.598
Zr–CA_{3H}	–0.745	–0.453	–0.723	–0.421	–0.713	–0.590	–0.563
	H14	**H15**	**H16**	**H17**	**H18**		
Ba–CA_{3H}	0.150	0.123	0.136	0.132	0.438		
Y–CA_{3H}	0.189	0.188	0.135	0.162	0.471		
Zr–CA_{3H}	0.228	0.232	0.177	0.193	0.504		

Table 5. Mulliken charges of the most stable metal–$EDTA_{4H}$ complexes

Complexes	Atom charges								
	O1	**O2**	**O3**	**O4**	**O5**	**O6**	**O7**	**O8**	**N9**
Ba–$EDTA_{4H}$	–0.640	–0.650	–0.643	–0.650	–0.629	–0.619	–0.627	–0.618	–0.359
Y–$EDTA_{4H}$	–0.535	–0.542	–0.536	–0.542	–0.623	–0.627	–0.623	–0.627	–0.501
Zr–$EDTA_{4H}$	–0.471	–0.483	–0.471	–0.483	–0.650	–0.653	–0.650	–0.653	–0.532
	C11	**C12**	**C13**	**C14**	**C15**	**C16**	**C17**	**C18**	**C19**
Ba–$EDTA_{4H}$	–0.138	–0.137	–0.208	–0.224	–0.206	–0.224	0.532	0.449	0.526
Y–$EDTA_{4H}$	–0.145	–0.145	–0.246	–0.239	–0.246	–0.239	0.561	0.572	0.561
Zr–$EDTA_{4H}$	–0.156	–0.156	–0.266	–0.246	–0.266	–0.246	0.593	0.603	0.593
	H21	**H22**	**H23**	**H24**	**H25**	**H26**	**H27**	**H28**	
Ba–$EDTA_{4H}$	0.113	0.143	0.106	0.151	0.095	0.159	0.092	0.129	
Y–$EDTA_{4H}$	0.173	0.183	0.173	0.183	0.171	0.205	0.170	0.199	
Zr–$EDTA_{4H}$	0.210	0.205	0.210	0.205	0.214	0.239	0.209	0.229	
	H29	**H30**	**H31**	**H32**	**H29**	**H30**	**H31**		
Ba–$EDTA_{4H}$	0.095	0.160	0.093	0.130	0.095	0.160	0.093		
Y–$EDTA_{4H}$	0.171	0.205	0.170	0.199	0.171	0.205	0.170		
Zr–$EDTA_{4H}$	0.214	0.239	0.209	0.229	0.214	0.239	0.209		

means, on average, the electron pair is found halfway between the two atoms and possesses similar negative charges. These results are consistent with results from Arivazhagan et al[42] that show higher electronegativity attracts more electrons and vice versa.

C1, C4, C6, and C7 in CA_{3H} and C17 to C20 in $EDTA_{4H}$ (shown in Tables 4 and 5) carry positive charges as they are bonded to O. O atoms have a higher electronegativity than C atoms, meaning an O bond more strongly attracts the bonding pair of electrons compared to a C atom. Consequently, the electron pair is pulled towards the O atom, making the carbon atom positively charged. The same is observed in H atoms. All H atoms have a positive charge. H18 in CA_{3H} has a higher positive charge than other H atoms as it is bonded to an O atom. This is confirmed in a recent study by Gangadhara and Krishnan.[43]

4. Conclusion

The density functional B3LYP method was used to investigate interactions between chelating agents and metal cations in forming a specific barium zirconate (BZY) compound. The aim of the study was to determine the preferred coordinaton sites for Ba^{2+}, Y^{3+}, and Zr^{4+} in CA_{3H} and $EDTA_{4H}$. The results show that CA_{3H} and $EDTA_{4H}$ can bind to the metal cations considered. The metal cations were observed to bind to the electron-rich sites of the chelating agents. Not all sites had the same binding energy, however. Moreover, different cations showed different bonding strengths. Based on the results, Zr^{4+} complexation was found to be the most stable compared to the other complexes. Ba^{2+} did not fully chelate to $EDTA_{4H}$, rendering Ba–$EDTA_{4H}$ the least stable complex. The greater binding energies of EDTA, alongside its ability to bind metals through four carboxyl and two amine groups, confirm its stronger chelating power with respect to CA.

5. References

1. J. Li, J.-L. Luo, K. T. Chuang, A. R. Sanger, *Electrochim. Acta.* **2008,** *53*, 37013707. **DOI:**10.1016/j.electacta.2007.12.020
2. D. Medvedev, A. Murashkina, E. Pikalova, A. Demin, A. Podias, P. Tsiakaras, *Prog. Mater. Sci.* **2013,** *60*, 72–129. **DOI:**10.1016/j.pmatsci.2013.08.001
3. N. A. Ibarahim, M. A. M. Ishak, A. Ramli, N. Osman, *Int. J. Ind. Chem.* **2014,** *5*, 1–6. **DOI:**10.1007/s40090-014-0018-4
4. W. G. Coors, In: C. Sikalidis (Ed.) Advances in Ceramics - Synthesis and Characterization, Processing and Specific Applications, CoorsTek, Inc., USA, **2011**, pp 479–498.
5. J. Tong, D. Clark, L. Bernau, A. Subramaniyan, R. O'Hayre, *Solid State Ionics.* **2010,** *181*, 1486–1498. **DOI:**10.1016/j.ssi.2010.08.022
6. A. B. Stambouli, E. Traversa, *Renew. Sustain. Energy Rev.* **2002,** *6*, 433–455. **DOI:**10.1016/S1364-0321(02)00014-X
7. Z. Wei, A. Chak-Tong, D. You-Wei, *Chin. Phys. B.* **2013,** *22*, 1–11. https://iopscience.iop.org/article/10.1088/1674-1056/22/5/057501/meta
8. N. G. Park, *Mater. Today.* **2015,** *18*, 65–72. **DOI:**10.1016/j.mattod.2014.07.007
9. U. Wang, 2014, https://www.wsj.com/articles/perovskite-offers-shot-at-cheaper-solar-energy-1411937799 (accessed: February, 2014)
10. N. A. Abdullah, N. Osman, S. Hasan, O. H. Hassan, *Int. J. Electrochem. Sci.* **2012,** *7*, 9401–9409. **DOI:**10.4028/www.scientific.net/AMR.896.112
11. N. A. Abdullah, S. Hasan, N. Osman, *J. Chem.* **2013,** *2013*, 1–7. **DOI:**10.1155/2013/908340
12. S. Liu, X. Tan, K. Li, R. Hughes, *Ceram. Int.* **2002,** *28*, 327–335. **DOI:**10.1016/S0272-8842(01)00098-0
13. Y. Tao, J. Shao, J. Wang, W. G. Wang, *J. Power Sources.* **2008,** *185*, 609–614. **DOI:**10.1016/j.jpowsour.2008.09.021
14. M. Motta, C. V. Deimling, M. J. Saeki, P. N. Lisboa-Filho, *J. Sol-Gel Sci. Technol.* **2008,** *46*, 201–207. **DOI:**10.1007/s10971-007-1673-0
15. A. Primikyri, G. Mazzone, C. Lekka, A. G. Tzakos, N. Russo, I. P. Gerothanassis, *J. Phys. Chem.* **2014,** *119*, 83–95. **DOI:**10.1021/jp509752s
16. M. Leopoldini, N. Russo, S. Chiodo, M. Toscano, *J. Agr. Food. Chem.* **2006,** *54*, 6343–6351. **DOI:**10.1021/jf060986h
17. A. Galano, G. Mazzone, R. Alvarez-Diduk, T. Marino, J. R. Alvarez-Idaboy, N. Russo, *Annu. Rev. Food Sci. Technol.* **2016,** *7*, 335–352. **DOI:**10.1146/annurev-food-041715-033206
18. Chemspider Search and Share Chemistry, 2014, https://www.chemspider.com/ (accessed: March, 2014)
19. M. J. Frisch, G. W. Trucks, H. B. Schlegel, G. E. Scuseria, M. A. Robb, J. R. Cheeseman, G. Scalmani, V. Barone, B. Mennucci, G. A. Petersson, H. Nakatsuji, M. Caricato, X. Li, H. P. Hratchian, A. F. Izmaylov, J. Bloino, G. Zheng, J. L. Sonnenberg, M. Hada, M. Ehara, K. Toyota, R. Fukuda, J. Hasegawa, M. Ishida, T. Nakajima, Y. Honda, O. Kitao, H. Nakai, T. Vreven, J. A. Montgomery, Jr., J. E. Peralta, F. Ogliaro, M. Bearpark, J. J. Heyd, E. Brothers, K. N. Kudin, V. N. Staroverov, R. Kobayashi, J. Normand, K. Raghavachari, A. Rendell, J. C. Burant, S. S. Iyengar, J. Tomasi, M. Cossi, N. Rega, M. J. Millam, M. Klene, J. E. Knox, J. B. Cross, V. Bakken, C. Adamo, J. Jaramillo, R. Gomperts, R. E. Stratmann, O. Yazyev, A. J. Austin, R. Cammi, C. Pomelli, J. W. Ochterski, R. L. Martin, K. Morokuma, V. G. Zakrzewski, G. A. Voth, P. Salvador, J. J. Dannenberg, S. Dapprich, A. D. Daniels, Ö. Farkas, J. B. Foresman, J. V. Ortiz, J. Cioslowski, D. J. Fox, Gaussian, Inc., Wallingford CT USA, 2009.
20. S. Grimme, J. Antony, S. Ehrlich, H. Krieg, *J. Chem. Phys.* **2010,** *132*, 1456–1465. **DOI:**10.1063/1.3382344
21. S. Grimme, S. Ehrlich, L. Goerigk, *J. Comput. Chem.* **2011,** *32*, 1456–1465. **DOI:**10.1002/jcc.21759
22. R. D. Dennington II, T. A. Keith, J. Millam, Semichem, Inc., USA, 2007.
23. T. Sakajiri, H. Yajima, T. Yamamura, *ISRN Biophys.* **2012,** *2012*, 1–5. **DOI:**10.5402/2012/124803
24. C. E. Housecroft, A. G. Sharpe, Inorganic Chemistry, Ashford

Colour Press Ltd., Gosport, London, UK, **2005**.
25. M. Satterfield, J. S. Brodbelt, *lnorg. Chem.* **2001,** *40*, 5393–5400. **DOI:**10.1021/ic010356r
26. N. F. Dalleska, K. Honma, L. S. Sunderlin, P. B. Armentrout, *J. Am. Chem. Soc.* **1994,** *116*, 3519–3528. **DOI:**10.1021/ja00087a044
27. T. Dudev, C. Lim, *J. Am. Chem. Soc.* **2013,** *114*, 538–556. **DOI:**10.1021/cr4004665
28. S. Bohm, E. Makrlik, P. Vanura, *Monatsh. Chem.* **2015,** *146*, 1229–1231. **DOI:**10.1007/s00706-014-1393-4
29. B. G. Johnson, C. A. Gonzales, P. M. W. Gill, J. A. Pople, *Chem. Phys. Lett.* **1994,** *221*, 100–108. **DOI:**10.1016/0009-2614(94)87024-1
30. E. Makrlik, P. Toman, P. Vanura, *J. Radioanal. Nucl. Chem.* **2013,** *295*, 1887–1891. **DOI:**10.1007/s10967-012-2107-1
31. M. P. Coles, P. B. Hitchcock, *Inorg. Chim. Acta.* **2004,** *357*, 4330–4334. **DOI:**10.1016/j.ica.2004.06.015
32. G. Vlaic, P. Fornasiero, S. Geremia, J. Kaspar, M. Graziani, *J. Catal.* **1997,** *168*, 386–392.
33. A. Kovacs, D. S. Nemcsok, T. Kocsis, *J. Mol. Struct.* **2010,** *950*, 93–97. **DOI:**10.1016/j.theochem.2010.03.036
34. N. Osman, N. A. Abdullah, S. Hasan, in: K. Junichi (Ed.), Thermal Decomposition and Phase Formation of Cerate-Zirconate Ceramics Prepared with Different Chelating Agents: Solid State Ionics: Ionics for Sustainable World - Proceedings of the 13th Asian Conference, **2013**, pp. 317–323.
35. N. Osman, N. A. Abdullah, S. Hasan, *Adv. Mater. Res. (Durnten-Zurich, Switz.)* **2014,** *896*, 112–115. **DOI:**10.4028/www.scientific.net/AMR.896.112
36. S. A. Thomas, J. F. Gaillard, *J. Phys. Chem.* **2015,** *119*, 2878–2884. **DOI:**10.1021/acs.jpca.5b00343
37. T. M. Suzuki, D. A. P. Tanaka, M. A. L. Tanco, M. Kanesato, T. Yokoyama, *J. Environ. Monit.* **2000,** *2*, 550–555. **DOI:**10.1039/B006738P
38. A. I. Pozhidaev, M. A. Porai-Koshits, T. N. Polynova, *J. Struct. Chem.* **1974,** *15*, 548–553. **DOI:**10.1007/BF00747194
39. F. Y. Adeowo, B. Honarparvar, A. A. Skelton, *RSC Adv.* **2016,** *6*, 79485–79496. **DOI:**10.1039/C6RA20203A
40. A. A. Skelton, N. Agrawal, J. R. Fried, *RSC Adv.* **2015,** *5*, 55033-55047. **DOI:**10.1039/C4RA14000A
41. F. Y. Adeowo, B. Honarparvar, A. A. Skelton, *J. Phys. Chem. A.* **2017,** *121*, 6054–6062. **DOI:**10.1021/acs.jpca.7b01017
42. M. Arivazhagan, S. Manivel, S. Jeyavijayan, R. Meenakshi, *Spectrochim. Acta. A. Mol. Biomol. Spectrosc.* **2015,** *134*, 493–501. **DOI:**10.1016/j.saa.2014.06.108
43. R. P. Gangadharan, S. Krishnan, *Acta Phys. Pol. A.* **2014,** *125*, 18–22. **DOI:**10.12693/APhysPolA.125.18

Povzetek

Z izračuni gostotnega funkcionala smo proučevali kovinske komplekse, ki nastanejo med sintezo barijevega cirkonata (BZY). Molekularne interakcije med tvorbo kompleksov ligand-kovin tekom te sinteze namreč niso znane. V tej študiji so bili izvedeni izračuni za določitev prednostnih koordinacijskih mest za kovinske komplekse. Katione Ba^{2+}, Y^{3+} in Zr^{4+} smo modelirali tako, da bi na strateških položajih interagirali z dvema deprotoniranima kelatnima reagentoma (citronska kislina [CA] in etilendiaminetetraocetna kislina [EDTA]). Uporabili smo teorijo gostotnega funkcionalna (DFT) na B3LYP nivoju z osnovnim 6-31G* in univerzalnim Gaussovim (UGBS) baznim setom. Iz dobljenih geometrijskih podatkov, veznih energij in porazdelitev naboja smo ugotovili, da lahko CA in EDTA vežeta proučevane kovinske katione, ki pa težijo k tvorbi vezi na mestih z večjo elektronsko gostoto. Od treh kovinskih kationov je bilo ugotovljeno, da najmočnejše vezi z deprotoniranim CA in EDTA tvori Zr^{4+}, sledi Y^{3+} in nato Ba^{2+}.